Novel Role of Tieg1 in Muscle Metabolism and Mitochondrial Oxidative Capacities

Malek Kammoun, Jérôme Piquereau, Vladimir Veksler, Lydie
Nadal-Desbarats, Sandra Même, Maud Beuvin, Gisèle Bonne, Yann Le Fur,
Philippe Pouletaut, William Même, et al.

HAL Id: hal-02304067
https://hal.utc.fr/hal-02304067v2

Submitted on 25 Jun 2021

Novel Role of *Tieg1* in Muscle Metabolism

and Mitochondrial Oxidative Capacities

Malek Kammoun[1], Jerome Piquereau[2], Lydie Nadal-Desbarats[3], Sandra Même[4], Maud Beuvin[5], Gisèle Bonne[5], Vladimir Veksler[2], Yann Le Fur[6], Philippe Pouletaut[1], William Même[4], Frederic Szeremeta[4], Jean-Marc Constans[7], Elizabeth S. Bruinsma[8], Molly H. Nelson Holte[8], Zeynab Najafova[9], Steven A. Johnsen[9], Malayannan Subramaniam[8], John R. Hawse[8,*] and Sabine F. Bensamoun[1,*]

[1]Alliance Sorbonne Universités, Université de Technologie de Compiègne, Biomechanics and Bioengineering Laboratory, UMR CNRS 7338, Compiègne, France

[2]Signalling and cardiovascular pathophysiology - UMR-S 1180, Université Paris-Sud, INSERM, Université Paris-Saclay, Châtenay-Malabry, France

[3]UMR 1253, iBrain, Université de Tours, Inserm, Tours, France

[4]Centre de biophysique Moléculaire, CNRS UPR4301, Orléans, France

[5]Sorbonne Université, Inserm U974, Centre de Recherche en Myologie, Paris France.

[6]Aix-Marseille Univ, CNRS, CRMBM, Marseille, France

[7]CHU Amiens, Institut Faire Faces, EA Chimère, Imagerie et Radiologie Médicale, Amiens, France

[8]Department of Biochemistry and Molecular Biology, Mayo Clinic, Rochester, MN USA

[9]Department of General, Visceral and Pediatric Surgery, University Medical Center Göttingen, 37075 Göttingen, Germany

*Corresponding author: Correspondence and requests for materials should be addressed to S. F. B. (Email: sabine.bensamoun@utc.fr) and J.R.H (Email: hawse.john@mayo.edu)

ABSTRACT

Aim: *Tieg1* is involved in multiple signaling pathways, human diseases, and is highly expressed in muscle where its functions are poorly understood.

Methods: We have utilized *Tieg1* KO mice to identify novel and important roles for this transcription factor in regulating muscle ultrastructure, metabolism and mitochondrial functions in the soleus and EDL muscles. RNA sequencing, immunoblotting, TEM, MRI, NMR, histochemical and mitochondrial function assays were performed.

Results: Loss of *Tieg1* expression resulted in altered sarcomere organization and a significant decrease in mitochondrial number. Histochemical analyses demonstrated an absence of SDH staining and a decrease in COX enzyme activity in KO soleus with similar, but diminished, effects in the EDL. Decreased complex I, COX and citrate synthase activities were detected in the soleus muscle of KO mice indicating altered mitochondrial function. Complex I activity was also diminished in KO EDL. Significant decreases in citrate synthase and respiratory chain complex activities were identified in KO soleus. ^{1}H-NMR spectra revealed no significant metabolic difference between WT and KO muscles. However, ^{31}P spectra revealed a significant decrease in phosphocreatine and ATPγ. Altered expression of 279 genes, many of which play roles in mitochondrial and muscle function, were identified in KO soleus muscle. Ultimately, all of these changes resulted in an exercise intolerance phenotype in *Tieg1* KO mice.

Conclusion: Our findings have implicated novel roles for *Tieg1* in muscle including regulation of gene expression, metabolic activity and organization of tissue ultrastructure. This muscle phenotype resembles diseases associated with exercise intolerance and myopathies of unknown consequence.

Keywords. *Tieg1*; *Klf10*; Skeletal Muscle; Mitochondria; Metabolism

INTRODUCTION

TGFβ inducible early gene-1 (*Tieg1*), also known as Krüppel-like factor 10 (*Klf10*), is a zinc finger-containing transcription factor known to be involved in multiple signaling pathways and disease processes [1,2]. *Tieg1* was originally discovered in human osteoblast cells as an early response gene following TGFβ treatment [3]. Clinically, altered expression levels of *Tieg1*, as well as single nucleotide polymorphisms (SNPs) in the *Tieg1* gene, are associated with osteoporosis in humans [4,5]. Further, SNPs in *Tieg1* have been identified in patients with hypertrophic cardiomyopathy [6]. Finally, decreased expression of *Tieg1* is observed during breast cancer progression [7,8] and SNPs in the *Tieg1* gene have been shown to predict risk of ovarian cancer [9].

Many of these clinical findings have been corroborated through the use of a *TIEG1* knockout mouse model system. Specifically, global deletion of *Tieg1* in mice results in an osteopenic skeletal phenotype [10,11], attenuates estrogen signaling in bone tissues [12,13] and leads to hypertrophy of the heart [14]. Further characterization of this gene has revealed a central role for *Tieg1* in regulating canonical Wnt signaling [15,16], TGFβ signaling [17-19] as well as BMP signaling [20-24] in multiple tissues and cell types.

As part of the original description and characterization of the *Tieg1* gene, it was shown to be most highly expressed in skeletal muscle [3]. However, little is known about its involvement in mediating the development, repair or function of this tissue. Recent studies performed by our group have shown that deletion of *Tieg1* in mice results in different functional responses of slow and fast twitch muscle fibers [25,26]. In parallel to these mechanical tests, imaging analyses (MRI, 9.4T) revealed changes in the texture profile between wild-type (WT) and *Tieg1* knockout (KO) mouse skeletal muscles [27]. Histochemical analyses demonstrated hyperplasia and hypertrophy of all fiber types in *Tieg1* KO muscles (soleus and extensor digitorum longus: EDL) with a significant increase in the percentage of glycolytic fibers and a decrease

in the percentage of oxidative fibers [25]. At the cellular level, others have implicated *Tieg1* in myogenic differentiation given its role in downstream regulation of myostatin and TGFβ signaling in myoblasts [28,29].

Here, we expand upon our previous studies to comprehensively characterize the skeletal muscle defects observed in *Tieg1* KO mice and to begin to elucidate the molecular mechanisms by which deletion of a single nuclear transcription factor results in a severe skeletal muscle phenotype that resembles multiple forms of mitochondrial-related myopathies in humans. Specifically, we have utilized RNA sequencing (RNAseq) to characterize the *Tieg1*-regulated transcriptome in skeletal muscle and have identified mis-regulation of multiple genes implicated in mitochondrial function and muscle biology. Given these findings, we have further characterized the role of *Tieg1* in skeletal muscle function and have identified significant defects with regard to mitochondrial oxidative capacities and metabolism in *Tieg1* KO skeletal muscle. The present experiments shed light on the hierarchy of molecular changes occurring in *Tieg1* KO muscles and enhance our understanding of muscle metabolism and mitochondrial oxidative capacities which are essential towards the goal of developing novel approaches for the treatment of myopathies and muscle-related diseases.

MATERIALS AND METHODS

Mice and Study design

The generation of *Tieg1* KO mice has been previously described [30] and initial characterization of *Tieg1* expression and function in skeletal muscle were previously reported [3,25,27]. For the studies presented here, littermate female animals from heterozygous breeding pairs were utilized and sacrificed for analysis at approximately 3 months of age. All mice were maintained in a temperature controlled room (22 ± 2°C) with light/dark cycle of 12 hours. Animals had free access to water and were fed with standard laboratory chow ad libitum. This study was carried out in strict accordance with the recommendations in the Guide for the Care and Use of Laboratory Animals of the National Institutes of Health. The protocol was approved by the French ministry of higher education, research and innovation (Permit Number: DUO-4776) and the Mayo Clinic Institutional Animal Care and Use Committee (Permit Number: A9615).

RNA isolation and sequencing

For the RNA sequencing studies, a total of 6 WT and 6 *Tieg1* KO mice were utilized. Immediately following sacrifice, the soleus muscle was dissected from mice, placed in trizol and sheared using an Ultra-Turrax homogenizer prior to extraction of total RNA using a miRNeasy Mini Kit (Qiagen, Germantown, MD). Total RNA was quantitated with a nanodrop and equal amounts of RNA from 2 individual WT or *Tieg1* KO mice were pooled to generate a total of 3 replicates per genotype. All samples were tested for RNA integrity before submitting for sequencing. mRNA sequencing was performed by the Mayo Clinic Molecular Biology Sequencing Core Facility using standard procedures. RNA libraries were prepared using 200 ng of good quality total RNA according to the manufacturer's instructions for the TruSeq RNA Sample Prep Kit v2 (Illumina, San Diego, CA) employing poly-A mRNA enrichment using oligo dT magnetic beads. The final adapter-modified cDNA fragments were

enriched by 12 cycles of PCR using Illumina TruSeq PCR primers. The concentration and size distribution of the completed libraries was determined using a Fragment Analyzer (AATI, Ankeny, IA) and Qubit fluorometry (Invitrogen, Carlsbad, CA). Libraries were sequenced at 40-50 million fragment reads per sample following Illumina's standard protocol using the Illumina cBot and HiSeq 3000/4000 PE Cluster Kit. The flow cells were sequenced as 100 X 2 paired end reads on an Illumina HiSeq 4000 using HiSeq 3000/4000 sequencing kit and HCS v3.3.52 collection software. Base-calling was performed using Illumina's RTA version 2.7.3.

RT-PCR

RNA was harvested from an additional 5 WT soleus and 8 EDL muscles as described above. One μg of RNA was reverse transcribed using the iScript™ cDNA Synthesis Kit (Bio-Rad, Hercules, CA) and real-time PCR was performed in triplicate for *Tieg1* and *β-Actin* using a Bio-Rad iCycler and a PerfeCTa™ SYBR Green Fast Mix™ for iQ real-time PCR kit (Quanta Biosciences, Gaithersburg, MD) as specified by the manufacturer. Cycling conditions were as follows: 95°C for 30 seconds followed by 40 cycles of 95°C for 3 seconds and 60°C for 30 seconds. Melt curves were generated to ensure amplification of a single PCR product. Quantitation of the PCR results was calculated based on the threshold cycle (C_t) following normalization to *β-Actin* and averaged among muscle type. PCR primers were designed using Primer3 software (http://frodo.wi.mit.edu/primer3/) and were purchased from Integrated DNA Technologies (Coralville, IA). Primer sequences were as follows: *Tieg1* F: GGGACAAAGCTGAGCAGAGT; *Tieg1* R: GGAAGCAAGCTGTCATCCTC; *β-Actin* F: AATCGTGCGTGACATCAAAGAG; *β-Actin* R: GCCATCTCCTGCTCGAAGTC.

Histochemical staining analysis

Soleus and EDL muscles were harvested from *Tieg1* KO (N=10) and WT (N=10) mice and immediately frozen in an isopentane bath that was cooled by liquid nitrogen and subsequently

7

stored at -80°C until the time of analysis. Ten μm serial sections were cut perpendicular to the muscle using a Microm HM 500M cryotome at -20°C. Analysis of succinate dehydrogenase (SDH), cytochrome c oxidase (COX) and menadione [31] were performed with histochemical staining to identify potential alterations in mitochondrial metabolism. Menadione is a quinone that is active during mitochondrial electron transport and has been reported to serve as an electron acceptor for several metalloproteins. The study of Wattenberg et al. [31] has demonstrated that menadione enhances the activity of SDH. Additionally, the endoplasmic reticulum (Dinitrophenylhydrazine), connective tissue (Gömöri trichrome), glycogen content (Periodic acid–Schiff) and lipid content (Oil Red O) were determined. Each staining procedure was performed using standard histochemical methods [32] on two independent tissue sections which were subsequently visualized under a Leica microscope using a 20 x objective. High-resolution images were captured with an Olympus cooled digital camera (DP-72) and interpretation of staining was based on the color histogram of the image using ImageJ software (US National Institutes of Health, Bethesda, MD, United States) [33]. This analysis separately measures the intensity in the red, green and blue channels of the image.

Transmission Electron Microscopy (TEM)

Prior to processing for TEM, the soleus (N=7) and the EDL (N=7) were dissected from WT and *Tieg1* KO mice with both extremities pinned to avoid muscle contraction and to maintain original length. Muscles were then immediately placed in fixative [1% (vol/vol) glutaraldehyde and 4% (vol/vol) paraformaldehyde in 0.1 M phosphate buffer, pH 7.2] [34] and incubated overnight at 4°C. Subsequently, two pieces (1 mm x 2 mm) of tissue were dissected from the middle of the tissue and rinsed for 30 min in three changes of 0.1 M phosphate buffer, pH 7.2, followed by a 1h secondary fixation in phosphate-buffered 1% OsO4 and 30 min in 1% uranyl acetate at room temperature. Following dehydration in a series of ethanol washes, tissue was embedded in EMbed 812 resin (EMS, Hatfield PA) and polymerized at

60°C for 18h [35]. Ultrathin (90 nm) sections were cut using a Leica UC7 ultramicrotome (Buffalo Grove, IL), placed on 200 mesh copper grids, and stained with lead citrate. Five micrographs of each specimen were randomly captured across the muscle tissue using a JEOL 1400Plus TEM (Peabody, MA), operating at 80 kV with a magnification of 42000x. ImageJ 1.46/Java 8 software (National Institute of Health, Bethesda, MD, United States) [33] was used to manually quantify the mitochondria area and the thick myofilament diameter.

Enzyme assays

Complete enzyme extractions from pieces of frozen soleus and EDL skeletal muscle tissue (N=7 WT, N=7 KO) were performed in an ice-cold buffer (50 mg ml^{-1}; containing (in mM): HEPES 5 (pH 8.7), EGTA 1, dithiothreitol 1, and 0.1% Triton X-100) using a Bertin Precellys 24 homogenizer (Bertin, Montigny-le-Bretonneux, France). Protein concentrations were assessed using the bicinchoninic acid assay. Total enzyme activities of citrate synthase (CS), mitochondrial NADH: coenzyme Q oxidoreductase (Complex I), mitochondrial succinic dehydrogenase (SDH, Complex II) and cytochrome oxidase (COX, Complex IV) were determined (30°C, pH 7.5) using standard spectrophotometric protocols as previously described [36,37]. Activities were reported as μmol min^{-1} / g protein (μmol min^{-1}, international units, IU). Mann Whitney tests were performed to compare enzyme activities as a function of genotype. A *P*-value < 0.05 was considered significant.

Mitochondrial respiration

Respiratory parameters of total mitochondrial populations were studied *in situ* in saponin-permeabilized fibers isolated from soleus and EDL muscles (N = 7 WT, N = 7 *Tieg1* KO). We followed the protocol described previously [38,39] using a Clark electrode (Strathkelvin Instruments, Glasgow, Scotland) in a water-jacketed oxygraphic cell filled with 3 ml of respiration solution containing Complex I substrates (10 mM glutamate + 4 mM malate) at

22°C with continuous stirring. Respiration rates were determined in the absence of ADP (basal respiration, Vo) and in the presence of a saturating (2 mM) ADP concentration. Functional activities of different complexes within the mitochondrial respiratory chain were estimated in the presence of succinate + amytal (or Amobarbital) to assess Complex II-supported respiration, and tetramethyl-p-phenylenediamine (TMPD) + ascorbate to assess the Complex IV-supported respiration. Respiration rates were expressed as μmol O_2 min^{-1} g^{-1} fiber dry weight. Mann Whitney tests were performed to compare mitochondrial respiration as a function of genotype. A P-value < 0.05 was considered significant.

Immunoblotting

Frozen soleus and EDL tissue samples from WT and *Tieg1* KO mice (N=6) were homogenized (Bertin Precellys 24) in ice cold buffer containing (in mM): HEPES 50 (pH=7.1), KCl, ethylenediaminetetraacetic acid (EDTA), β-glycerophosphate, orthovanadate 1, dithithreitol 1, sodium fluoride 50, Na pyrophosphate 5, phenylmethylsulfonyl fluoride 0.2 and an anti-protease cocktail (Calbiochem 539134) in the presence of Triton X-100 0.1%. Equal amounts of protein extracts were separated on SDS-polyacrylamide gels (10 to 12%) and transferred to polyvinylidene difluoride membranes for Western blotting. After 1h of blocking in PBS containing TWEEN20 (0.1%) and nonfat milk (5%), the membranes were incubated overnight at 4°C with primary antibodies (mitochondrial OXPHOS (complex I subunit NDUFB8, complex II subunit CII 30, complex III sunbunit core 2 and complex V subunit alpha): MS604 (mitosciences), Citrate synthase: ab96600 (Abcam), COX IV: ab14744 (Abcam), MFN2: H00009927-MO1 (Abnova), PGC-1α: sc13067 (Santa Cruz), OPA1: 612606 (Becton Dickinson), DRP1: 611112 (BD Biosciences). Oxyblot™protein oxidation detection kit (Millipore S7150) was used for protein carbonylation assessment. After washing, the membranes were incubated with secondary antibodies coupled with

horseradish peroxidase for 1h at room temperature and visualized using chemiluminescent substrate (Luminata[TM] Western Chemiluminescent HRP Substrates, Millipore). Light emission was detected by autoradiography and quantified using an image-analysis system (Bio-Rad). Mann Whitney tests were performed to compare protein abundance as a function of genotype. A *P*-value < 0.05 was considered significant.

In vivo Magnetic Resonance Spectroscopy

Twenty four mice were used (N=12 WT and N=12 *Tieg1* KO) for magnetic resonance (MR) acquisitions that were performed on a 9.4 Tesla Biospec 94/21 superconducting magnet (Bruker, Wissembourg, France) with a shielded gradient set (950 $mT.m^{-1}$ maximum gradient amplitude). A home built homogeneous scroll double tuned coil (10 mm inner diameter) was developed. The resonance frequencies were 400 MHz for the proton and 162 MHz for the phosphorus. Animals were anesthetized by inhalation of 2.5% isoflurane then maintained during MR experiments at 1.5% (0.5 $L.min^{-1}$ mixed in air and oxygen with 1:1 ratio). The physiological body temperature was maintained inside the magnet by circulating warm water. A pressure sensor was used to monitor the respiration cycle and obtain the respiration frequency.

Localized ^1H spectroscopy was performed with a PRESS (point resolved spectroscopy) sequence (TE/TR, 16 ms/4000 ms, 256 accumulations, 17min) with VAPOR module (variable pulse power and optimized relaxation delays) for water suppression. A 22 mm^3 voxel was centered on the middle of the hindlimb.

^{31}P spectroscopy was then performed with a PRESS sequence (TR = 1500ms, 1 pulse BP of 100µs 200 accumulations, DS = 2, TA = 5min). Due to the lack of sensitivity of ^{31}P spectroscopy the entire hindlimb was used for the acquisition ($1000mm^3$).

Spectra were analyzed with a homemade (CRMBM, Aix Marseille university) CSIAPO software used for quest interface [40] that works in time domain. On a ^{1}H spectrum the assessment of choline, creatine, taurine and extramyocellular lipids were made. On a ^{31}P spectrum, different metabolites are quantifiable: Inorganic phosphate, phosphocreatine, ATPα, ATPβ and ATPγ. Quantification of the area under peaks was performed in arbitrary units (AU). A Mann Whitney statistical test was used to compare those areas between both muscle genotypes.

^{1}H-NMR Metabolomics

The protocol for extraction of metabolites from soleus (N=18) and EDL (N=18) muscles was adapted from the Folch type two-step procedure described by Wu et al. [41] for sample mass < 50 mg. Prior to NMR analysis, dried samples were reconstituted in 220µL of deuterated buffer containing TSP [3-trimethylsilylpropionic acid] at 145µM and transferred to conventional 3mm NMR tubes (CortecNet, Paris, France). ^{1}H-NMR spectra were obtained with a Bruker DRX-600 AVANCE-III HD spectrometer (Bruker SADIS, Wissembourg, France), operating at 14 T, with a TCI cryoprobe. Standard water suppressed ^{1}H-NMR spectra were acquired at 298K using a "noesypr1d" pulse sequence with relaxation delay of 20s. Spectra were processed using Topspin version 3.2 software (Bruker Daltonik, Karlsruhe, Germany). ^{1}H-NMR spectra were automatically reduced to ASCII files using AMIX Software package (Analysis of MIXture, version 3.9.14, Bruker Biospin, Karlsruhe, Germany) as previously described [42]. Spectral intensities were scaled to the total spectral intensity and the resulting data (supplementary data S1 A-B) was analyzed by multivariate and univariate statistical analyses.

Multivariate and Univariate analysis

Principal Component Analyses (PCA) and Partial Least Square Discriminant Analyses (PLS-DA) were performed using SIMCA-P^{+} Software (version 13.0, Umetrics, Umeå, Sweden) on

the NMR dataset containing soleus and EDL as a function of genotype. All data sets were scaled to unit of variance allowing all metabolites to become equally important. PCA describes the total variability within the dataset and can be used as an informative indicator while the PLS-DA is used to predict the spectral features (metabolites) that define separation between groups (phenotypes) [43]. The overall quality of the models was judged by cumulative R^2 (goodness of fit) and cumulative Q^2 (goodness of prediction). Variable Importance in the Projection (VIP) > 1 were considered as the most contributive in the genotype separation. Student's *t-test* were performed using MetaboAnalyst [44] for all VIP measures. A *P*-value < 0.05 was considered significant.

Following statistical analysis, heatmaps were generated to visually depict changes in metabolites (VIP > 1 and a P-value < 0.05) as a function of mouse genotype (Supplementary data S1 A-B).

Bioinformatic analysis

The FASTQ files were mapped to the mouse genome (assembly mm9) using TopHat Gapped-read mapper [45] with very sensitive Bowtie2 settings on Galaxy Platform (version 2.1.0) [46]. The read counting was performed via HTSeq [47] (version 0.6.1galaxy3) with the following parameters: -f bam -r name -s no -a 10 -t exon -m union. The count files were subsequently subjected for differential analysis using the DESeq2 Package [48] on R (Bioconductor version 3.4.1). The threshold values to determine the differentially expressed genes were as follows: abs (log2fold change) $\geq$ 0.8 and padj < 0.05. The pathway analysis on the regulated genes was performed using "Enrichr" [49,50].

Treadmill exercise

The physical function of WT and *Tieg1* KO mice was assessed using a motorized treadmill (Columbus Instruments, Columbus, OH) test of exercise ability. Briefly, 15 WT and 15 *Tieg1* KO female mice are acclimated to the treadmill for 2 consecutive days immediately followed

by a test day. Acclimation consisted of 5 minutes of running at a speed of 5 m per minute for the first two minutes, 7 m per minute for the next 2 minutes and 9 m per minute for the last minute at an incline grade of 5%. For the test, mice ran on the treadmill to exhaustion with a 5% incline and starting speed of 5 m per minute for two minutes. The speed was increased by 2 m per minute every two minutes until the mice were exhausted. Exhaustion was defined as the inability of a mouse to stay on the treadmill in spite of a mild electrical stimulus and mechanical prodding. Total distance run was recorded for each mouse and group averages were calculated. Mann Whitney test were performed to compare the total distance run between genotypes. A *P*-value < 0.05 was considered significant.

RESULTS

Gene expression profile changes in *Tieg1* KO muscles

Given the morphological and functional changes observed in the skeletal muscles of *Tieg1* KO mice [25,27], we sought to elucidate *Tieg1*-dependent molecular mechanisms controlling skeletal muscle maintenance and function. We first assessed the expression levels of *Tieg1* in soleus and EDL muscle isolated from WT female mice. *Tieg1* expression was shown to be approximately 4-fold higher in soleus muscle compared to EDL muscle (Figure 1A). In light of these results, we next assessed the transcriptome-wide effect of *Tieg1* loss in the soleus of 12 week old mice (Figure 1B - 1C). In total, 279 genes were differentially regulated between the WT and *Tieg1* KO muscle (Figure 1D). Although the number of downregulated genes were substantially fewer, the pathway analyses indicated that a number of these genes are known targets of the *Myod1* transcription factor (Supplementary data, S2) which was shown to be upregulated in the muscle of *Tieg1* KO mice ($Log_2FC=1.46$, $p_{adj}=3.06E-16$). Interestingly, some of the downregulated genes (*Pln, Tfcp2l1, Ide, Bcl2l1*) are also known components of mitochondria (Supplementary data, S2) whereas most of the upregulated genes were associated with collagen and extracellular matrix organization (Supplementary data, S3).

Mitochondrial metabolism deficiencies in *Tieg1* KO muscles

Given the importance of mitochondrial function in skeletal muscle, we next histologically assessed the activity of some complexes of the mitochondrial electron transfer chain within muscle biopsies of WT and *Tieg1* KO mice. Remarkably, as shown in Figure 2A - 2B, SDH staining was completely absent in soleus muscle of *Tieg1* KO mice while normal staining patterns were observed in WT littermates. In addition, COX (Figure 2C - 2D) and menadione (Figure 2E - 2F) staining was less intense in *Tieg1* KO mice compared to WT controls. No significant differences in the staining for endoplasmic reticulum, connective tissue, glycogen content or lipids were observed (Figure 2G - 2L). Decreased staining for SDH, COX and

menadione were also observed in the EDL muscle of *Tieg1* KO mice, albeit to a lesser degree (Figure 3).

Disorganization of *Tieg1* KO muscle ultrastructure

Given the observed differences in staining patterns for important mitochondrial enzymes, we next sought to analyze the ultrastructure of the soleus and EDL muscle fibers using TEM. Longitudinal sections revealed disorganization of the muscle structure, and were suggestive of a contracted phenotype, in both *Tieg1* KO soleus and EDL muscles (Figure 4) compared to WT littermates. Specifically, smaller sarcomere lengths (1.5μm for KO and 2.5μm for WT), disappearance of the I band, shortening of the H band and changes in the shape of mitochondria where observed in *Tieg1* KO soleus (Figure 4D) and EDL muscles (Figure 4J). The quantification of mitochondrial area (A) revealed a significant ($P < 0.001$) decrease for soleus and EDL *Tieg1* KO muscles ($A_{WT\_soleus} = 0.079 \pm 0.003$ μm^2 vs $A_{Tieg1\ KO\_soleus} = 0.054 \pm 0.002$ μm^2 and $A_{WT\_EDL} = 0.08 \pm 0.003$ μm^2 vs $A_{Tieg1\ KO\_EDL} = 0.045 \pm 0.002$ μm^2). Mitochondrial area was classified within different ranges based on Picard's study [51] and a non-Gaussian curve was observed in both muscles with smaller mitochondria ($A_{soleus} < 0.04$ μm^2: 37% vs 14% and $A_{EDL} < 0.04$ μm^2: 58% vs 23%), and a complete absence of mitochondria with an area greater than 0.15 μm^2, in *Tieg1* KO mice.

Changes in mitochondrial activity in *Tieg1* KO muscle

A significant decrease in citrate synthase (CS) and respiratory chain complex activities were observed in *Tieg1* KO soleus muscle (Figure 5A - 5C). This result is in agreement with the decreased area occupied by mitochondria and the weaker COX and SDH staining (Figure 2) observed in *Tieg1* KO soleus fibers. No significant changes were observed for COX and CS activities in *Tieg1* KO EDL muscle (Figure 5D and 5F). However, NADH: ubiquinone oxidoreductase (Complex I) (Figure 5B and 5E) activity was decreased in both *Tieg1* KO soleus and EDL muscles.

Respiration rates of total mitochondrial populations using substrates for complexes I, II and IV were markedly lower in permeabilized *Tieg1* KO soleus muscle (Figure 6A) compared with WT controls. In contrast, mitochondria in *Tieg1* KO EDL muscle did not exhibit any differences in respiration (Figure 6B) as compared with WT. These results are in agreement with the enzyme activities showing a significant decrease only for the *Tieg1* KO soleus.

In soleus, protein content (Figure 7) of all complexes measured (I, II, III, V) was slightly lower in *Tieg1* KO muscle though these changes did not reach statistical significance except for complex IV (COX). No significant differences were observed for the protein of mitochondrial fusion (OPA1), mitofusin2 (Mfn2) as well as mitochondrial fission (DRP1) and biogenesis (PGC1-α) in the soleus muscle. For the EDL muscle, no significant differences were observed for any of these proteins between WT and *Tieg1* KO mice. Total protein carbonylation was determined to assess oxidative stress in skeletal muscles. No significant difference in the levels of oxidative stress were detected between WT and *Tieg1* KO soleus or EDL muscles (Figure 8).

Lack of *Tieg1* induces metabolic changes

[1]H spectra showed no significant difference for choline, creatine, taurine and extramyocellular lipids between WT and *Tieg1* KO muscle (Figure 9B). However, ^{31}P spectra revealed a significant difference in the levels of phosphocreatine and ATPγ (Figure 10B). The PCA model obtained with the ^{1}H-NMR data set containing WT soleus, *Tieg1* KO soleus, WT EDL and *Tieg1* KO EDL revealed significant separation between soleus and EDL muscles (PC1) explaining 50% of the total variability within the dataset (Figure 11). Mouse genotype (PC2) explained 24% of the total variability within the data (Figure 11). These results highlight differences between WT and *Tieg1* KO metabolic profiles.

PLS-DA models obtained with ^{1}H-NMR datasets from soleus muscles (Supplementary data, S1 A, predictive ability Q^2=0.72, goodness of fit R^2Y(cum)=0.99) and EDL muscles

(Supplementary data S1 B, predictive ability Q^2=0.84, goodness of fit R^2Y(cum)=0.99) revealed a clear separation between WT and KO genotypes regardless of muscle type suggesting that deletion of *Tieg1* results in significant changes in the metabolic profiles of skeletal muscle. The PLS-DA models allow for the identification of very important metabolites in projection (VIPs) whose changes are likely to be biologically relevant (Supplementary data, S4). Figure 12 depicts heatmaps (12A for soleus muscle, 12B for EDL muscle) generated for metabolites with a VIP > 1 in the PLS-DA models. For both *Tieg1* KO soleus and EDL muscles, there were more down regulated metabolites compared to WT muscles. Of note, there were differences in the metabolites that were identified to be differentially regulated by loss of *Tieg1* expression between the two muscle types.

Loss of *Tieg1* expression results in exercise intolerance

In light of the many defects observed in *Tieg1* KO skeletal muscle including gene expression changes, muscle ultrastructure and mitochondrial activity and metabolism, we sought to determine if these defects impacted muscle function *in vivo*. Treadmill exercise tests were performed to determine the distance run prior to exhaustion. These tests revealed significant decreases in the distance run by *Tieg1* KO mice compared to WT littermates (Figure 13). On average, WT mice ran 309 m prior to exhaustion while *Tieg1* KO mice ran only 214 m equating to an approximately 25% decrease in exercise ability (Figure 13).

DISCUSSION

We have previously shown that deletion of the *Tieg1* gene in mice results in muscle fiber hypertrophy, glycolytic fiber type switching, texture profile changes and defects in the functional properties of skeletal muscle [25]. Here, we have expanded upon these original discoveries to further investigate the molecular and cellular basis for the observed skeletal muscle defects. Specifically, we have shown that *Tieg1* plays a central role in regulating mitochondrial oxidative capacities and metabolism.

Through gene expression profiling, we observed up-regulation of the *Myod1* "myogenic differentiation 1" gene in *Tieg1* KO muscles. This gene is well known to be a regulator of myogenic differentiation [52-54] and its mis-regulation may contribute to the observed muscle fiber hypertrophy in *Tieg1* KO mice. However, this assumption must be confirmed by additional experiments to identify the exact connection between *Tieg1* and *Myod1*. Moreover, a disorganization of the muscle ultrastructure and a contracted phenotype were observed in *Tieg1* KO skeletal muscle as defined by smaller sarcomeres, the absence of I bands and the shortening of H bands. Unger's group showed that chaperone proteins were capable of aggregating and binding to titin filaments resulting in shorter sarcomeres in hereditary myopathies (Duchenne, Titinopathy, etc …) [55]. However, RNAseq analysis did not identify significant differences in *Hsp* expression levels and it will be of interest to quantify the abundance of HSPs in *Tieg1* KO muscle in future studies.

Pathway analyses of genes identified to be differentially expressed in *Tieg1* KO skeletal muscle revealed alterations in the expression levels of 48 genes that are known to be related to muscle diseases (such as Duchenne muscular dystrophy, Becker muscular dystrophy, etc …). Interestingly, the genes implicated in these muscle diseases were primarily collagens (*Col1a1, Col1a2, Col5a1, Col6a2*, etc …) which were all upregulated in *Tieg1* KO mice. A study by Bönnemann et al. has previously shown that collagen VI-related myopathies encompass a

spectrum of diseases ranging from severe Ullrich muscular dystrophy to mild Bethlem myopathy [56]. Moreover, it has been demonstrated that *Col1a1* is the most commonly evaluated collagen gene for fibrosis [57], and our results are also in agreement with DiMario's study showing an increase of *Col1a1* gene expression, and protein content, in *Tieg1* KO muscle (tibialis anterior and diaphragm) [58]. In addition, this phenomenon is more accentuated in the *Tieg1* KO/mdx (Duchenne muscular dystrophy) mouse model [58].

Tieg1 KO mice also exhibit increased expression of TGFβ within the skeletal muscle. We have specifically demonstrated that *Tieg1* represses the expression of *Smad* 7 [17] and induces the expression of *Smad* 2 [18]. We have also shown that over-expression of *Tieg1* mimics the effects of TGFβ treatment in multiple cell types [59]. Overall, we have shown that *Tieg1* serves as a positive feedback loop for TGFβ signaling. Based on these previous observations, it is possible that increased expression of TGFβ in the soleus of *Tieg1* KO mice is a compensatory mechanism for diminished TGFβ pathway activity in the absence of *Tieg1* expression. Similar results were observed after muscle rotator cuff tears in a rat model which results in a significant increase of fibrosis and muscular dystrophy. To explain this phenomenon, Liu et al [60] have linked TGFβ to the Akt/mTOR pathway and suggest that TGFβ may be the primary factor regulating muscle changes after muscle rotator cuff tears. In general, TGFβ pathways are highly conserved pathways that exert a potent level of control over muscle gene expression and are critical regulators of fibrosis in multiple organ systems.

In addition to muscular dystrophy, mitochondrial myopathy pathways were also identified from the gene expression data. For instance, Rmrp (RNA component of mitochondrial RNAase P) was identified in these pathways and was significantly down-regulated in *Tieg1* KO soleus muscle. The decreased expression of mitochondrial complex proteins have confirmed the involvement of *Tieg1* with regard to mitochondrial oxidative capacities and may explain some of the structural and functional changes of the mitochondria observed in

Tieg1 KO muscle. These mitochondrial disease are also related to another disease called "mitochondrial complex I deficiency". In the present study, complex I activity and respiration were found to be decreased in *Tieg1* KO muscle, further demonstrating an important role for *Tieg1* in mitochondrial activity and function. Such a specific impairment of complex I function has been observed in several diseases including cardiomyopathy and heart failure [61,62]. Indeed, complex I specific and functional activities could be decreased, when other ETC (electron transport chain) complexes or total mitochondrial mass (usually estimated by citrate synthase activity) are normal. This is the case, for example, in generalized myopathy in advanced heart failure [63]. Similarly, complex I in skeletal muscle mitochondria is the primary target of the immunosuppressive molecule cyclosporine toxicity [64]. A marked decrease in complex I activity was found in skeletal muscle in acute intermittent porphyria (a disease primarily affecting the nervous system), an autosomal dominant metabolic disease [65]. Such a specific inhibition of complex I has an important impact on mitochondrial function in striated muscle since this complex is the rate limiting step of the electron flux through the ETC.

Similarly, deficiencies in SDH (Succinate dehydrogenase) have been reported in human mitochondrial diseases [66-68]. Haller et al. have reported on a 22 year old man with life-long exercise intolerance marked by premature fatigue [67]. Additionally, Kollberg et al. described a 77 year old woman with muscle fatigue and dyspnea resulting from SDH deficiency [66]. Moreover, Vladutiu et al. have assessed qualitative and quantitative SDH expression in muscle biopsies from 108 patients (age range: 1 to 68 years) with mitochondrial myopathies [68] exhibiting muscle pain, exercise intolerance and cardiomyopathy, etc. As is the case with *Tieg1* KO mice as reported here, a decrease in all respiratory chain complexes was associated with a deficiency of SDH activity (23% of patients) showing an important reduction for 12 patients. The results reported in these clinical studies have described skeletal muscle disorders

resulting from mitochondrial defects closely resembling the muscle phenotype of *Tieg1* KO mice.

Oxygen consumption rate and the enzyme activity analyses reflect clear decreases in *Tieg1* KO muscle, whereas the protein content of respiratory chain complexes do not (though all complexes do exhibit a slight but non-significant decrease). Indeed, the respiration rates do not depend only on absolute mitochondrial protein content, but rather are a function of numerous enzyme activities, lipid environment, inner membrane properties etc. Even specific enzyme activities do not exactly reflect the enzyme protein content. Moreover, mitochondrial complexes represent structures formed by various subunits. Generally, the antibodies against one subunit do not necessarily reveal protein content of the whole complex. It is for these reasons that investigation of mitochondrial function requires the complete analysis of oxygen consumption rates and specific enzyme activities in addition to protein content determination in order to fully understand the basis for a given mitochondrial defect. The same rationale concerns the SDH staining. This method determines SDH activity rather than SDH protein content. Moreover, the staining reveals the enzyme activity in situ rather than specific activity of purified SDH. The results obtained show that *Tieg1* deficiency primarily alters the functional properties of mitochondrial proteins rather than their expression levels.

Interestingly, we have observed that loss of *Tieg1* expression has a strong muscle-type specific effect in that, the soleus is more affected than that of the EDL. The differences in the severity of this muscle phenotype between the soleus and EDL may be due to the observed higher expression of *Tieg1* in WT soleus muscle compared to WT EDL muscle. It will be of interest to further characterize the glycolytic switch of oxidative muscle. These observations are in agreement with DiMario's study where loss of *Tieg1* expression resulted in a pronounced fibrotic phenotype in slow twitch (diaphragm) muscle compared to fast twitch muscle (tibialis anterior) [58]. However, through ^{1}H-NMR metabolic profiling, we have shown

that both slow and fast twitch muscles are affected by deletion of *Tieg1*. Metabolites such as fumarate, lactate and pyruvate were up-regulated in *Tieg1* KO EDL muscle. These metabolites are involved in the Krebs cycle and reflect alterations in mitochondria metabolism. Nicotinurate was up-regulated, and beta-hydroxy-butyrate was down-regulated, in both muscles of *Tieg1* KO mice. Nicotinurate is used to diagnose disorders associated with mitochondrial fatty acid beta-oxidation and beta-hydroxy-butyrate, a ketone body, which is produced by beta-oxydation as an energy source. Furthermore, in vivo ^{31}P-NMR spectroscopy revealed decreased ATP (adenosine triphosphate) and PCr levels that are involved in energy metabolism, again implicating an important role for *Tieg1* in mitochondrial function. The amino-acids valine, leucine, lysine and glutamate were also shown to be down-regulated in both soleus and EDL muscles and are associated with protein metabolism. This metabolic imbalance in both *Tieg1* KO muscle types can be related to mitochondrial pathways confirming the strong implication of the *Tieg1* gene in the function and activity of mitochondria.

The present study has demonstrated a new role for *Tieg1* in the regulation of skeletal muscle energy metabolism, specifically in oxidative muscle which strongly depends on mitochondrial function. The observed differences in mitochondrial activity could in part be explained by the known fiber type switching that occurs in *Tieg1* KO mice [25]. Thus, the *Tieg1* KO mice mimic human diseases associated with muscle fatigue and exercise intolerance and could allow for the study of mitochondrial myopathies associated with deficiency of SDH in skeletal muscle. Indeed, we have demonstrated that loss of TIEG expression results in an exercise intolerance phenotype in mice that is likely explained by the many defects in mitochondrial function described here. For these reasons, *Tieg1* KO mice represent a novel model for further understanding muscle pathologies and mitochondrial dysfunction. These findings have laid the groundwork for future efforts aimed at identifying specific genes and their associated

pathways that can be pharmacologically manipulated to reverse/alleviate these defects in *Tieg1* KO mice and to evaluate their efficacy for the treatment of muscle disorders in humans.

ACKNOWLEDGMENTS

CONFLICT OF INTEREST

The authors declare no competing interests.

REFERENCES

1. Subramaniam M, Hawse JR, Rajamannan NM, Ingle JN, Spelsberg TC. Functional role of KLF10 in multiple disease processes. *Biofactors.* 2010;36(1):8-18.

2. Hawse JR, Subramaniam M, Ingle JN, Oursler MJ, Rajamannan NM, Spelsberg TC. Estrogen-TGFbeta cross-talk in bone and other cell types: role of TIEG, Runx2, and other transcription factors. *Journal of cellular biochemistry.* 2008;103(2):383-392.

3. Subramaniam M, Harris SA, Oursler MJ, Rasmussen K, Riggs BL, Spelsberg TC. Identification of a novel TGF-beta-regulated gene encoding a putative zinc finger protein in human osteoblasts. *Nucleic acids research.* 1995;23(23):4907-4912.

4. Yerges LM, Klei L, Cauley JA, et al. Candidate gene analysis of femoral neck trabecular and cortical volumetric bone mineral density in older men. *Journal of bone and mineral research : the official journal of the American Society for Bone and Mineral Research.* 2010;25(2):330-338.

5. Hopwood B, Tsykin A, Findlay DM, Fazzalari NL. Gene expression profile of the bone microenvironment in human fragility fracture bone. *Bone.* 2009;44(1):87-101.

6. Bos JM, Subramaniam M, Hawse JR, et al. TGFbeta-inducible early gene-1 (TIEG1) mutations in hypertrophic cardiomyopathy. *Journal of cellular biochemistry.* 2012;113(6):1896-1903.

7. Subramaniam M, Hefferan TE, Tau K, et al. Tissue, cell type, and breast cancer stage-specific expression of a TGF-beta inducible early transcription factor gene. *Journal of cellular biochemistry.* 1998;68(2):226-236.

8. Reinholz MM, An MW, Johnsen SA, et al. Differential gene expression of TGF beta inducible early gene (TIEG), Smad7, Smad2 and Bard1 in normal and malignant breast tissue. *Breast Cancer Res Treat.* 2004;86(1):75-88.

9.   Jim HS, Lin HY, Tyrer JP, et al. Common Genetic Variation in Circadian Rhythm Genes and Risk of Epithelial Ovarian Cancer (EOC). *J Genet Genome Res.* 2015;2(2).

10.   Bensamoun SF, Hawse JR, Subramaniam M, et al. TGFbeta inducible early gene-1 knockout mice display defects in bone strength and microarchitecture. *Bone.* 2006;39(6):1244-1251.

11.   Hawse JR, Iwaniec UT, Bensamoun SF, et al. TIEG-null mice display an osteopenic gender-specific phenotype. *Bone.* 2008;42(6):1025-1031.

12.   Hawse JR, Pitel KS, Cicek M, et al. TGFbeta inducible early gene-1 plays an important role in mediating estrogen signaling in the skeleton. *Journal of bone and mineral research : the official journal of the American Society for Bone and Mineral Research.* 2014;29(5):1206-1216.

13.   Hawse JR, Subramaniam M, Monroe DG, et al. Estrogen receptor beta isoform-specific induction of transforming growth factor beta-inducible early gene-1 in human osteoblast cells: an essential role for the activation function 1 domain. *Mol Endocrinol.* 2008;22(7):1579-1595.

14.   Rajamannan NM, Subramaniam M, Abraham TP, et al. TGFbeta inducible early gene-1 (TIEG1) and cardiac hypertrophy: Discovery and characterization of a novel signaling pathway. *Journal of cellular biochemistry.* 2007;100(2):315-325.

15.   Subramaniam M, Cicek M, Pitel KS, et al. TIEG1 modulates beta-catenin sub-cellular localization and enhances Wnt signaling in bone. *Nucleic acids research.* 2017;45(9):5170-5182.

16.   Subramaniam M, Pitel KS, Bruinsma ES, Monroe DG, Hawse JR. TIEG and estrogen modulate SOST expression in the murine skeleton. *Journal of cellular physiology.* 2018;233(4):3540-3551.

17. Johnsen SA, Subramaniam M, Janknecht R, Spelsberg TC. TGFbeta inducible early gene enhances TGFbeta/Smad-dependent transcriptional responses. *Oncogene.* 2002;21(37):5783-5790.

18. Johnsen SA, Subramaniam M, Katagiri T, Janknecht R, Spelsberg TC. Transcriptional regulation of Smad2 is required for enhancement of TGFβ/Smad signaling by TGFβ inducible early gene. *Journal of cellular biochemistry.* 2002;87(2):233-241.

19. Johnsen SA, Subramaniam M, Monroe DG, Janknecht R, Spelsberg TC. Modulation of transforming growth factor beta (TGFbeta)/Smad transcriptional responses through targeted degradation of TGFbeta-inducible early gene-1 by human seven in absentia homologue. *The Journal of biological chemistry.* 2002;277(34):30754-30759.

20. Hefferan TE, Subramaniam M, Khosla S, Riggs BL, Spelsberg TC. Cytokine-specific induction of the TGF-beta inducible early gene (TIEG): regulation by specific members of the TGF-beta family. *Journal of cellular biochemistry.* 2000;78(3):380-390.

21. Subramaniam M, Pitel KS, Withers SG, Drissi H, Hawse JR. TIEG1 enhances Osterix expression and mediates its induction by TGFbeta and BMP2 in osteoblasts. *Biochemical and biophysical research communications.* 2016;470(3):528-533.

22. Hawse JR, Cicek M, Grygo SB, et al. TIEG1/KLF10 modulates Runx2 expression and activity in osteoblasts. *PloS one.* 2011;6(4):e19429.

23. Yadav PS, Khan MP, Prashar P, et al. Characterization of BMP signaling dependent osteogenesis using a BMP depletable avianized bone marrow stromal cell line (TVA-BMSC). *Bone.* 2016;91:39-52.

24. Prashar P, Yadav PS, Samarjeet F, Bandyopadhyay A. Microarray meta-analysis identifies evolutionarily conserved BMP signaling targets in developing long bones. *Developmental biology.* 2014;389(2):192-207.

25. Kammoun M, Pouletaut P, Canon F, et al. Impact of TIEG1 Deletion on the Passive Mechanical Properties of Fast and Slow Twitch Skeletal Muscles in Female Mice. *PloS one.* 2016;11(10):e0164566.

26. Kammoun M, Ternifi R, Dupres V, et al. Development of a novel multiphysical approach for the characterization of mechanical properties of musculotendinous tissues. *Scientific reports.* 2019;9(1):7733.

27. Kammoun M, Meme S, Meme W, et al. Impact of TIEG1 on the structural properties of fast and slow twitch skeletal muscle. *Muscle Nerve.* 2016.

28. Miyake M, Hayashi S, Iwasaki S, et al. Possible role of TIEG1 as a feedback regulator of myostatin and TGF-beta in myoblasts. *Biochemical and biophysical research communications.* 2010;393(4):762-766.

29. Miyake M, Hayashi S, Iwasaki S, et al. TIEG1 negatively controls the myoblast pool indispensable for fusion during myogenic differentiation of C2C12 cells. *Journal of cellular physiology.* 2011;226(4):1128-1136.

30. Subramaniam M, Gorny G, Johnsen SA, et al. TIEG1 null mouse-derived osteoblasts are defective in mineralization and in support of osteoclast differentiation in vitro. *Molecular and cellular biology.* 2005;25(3):1191-1199.

31. Wattenberg LW, Leong JL. Effects of coenzyme Q10 and menadione on succinic dehydrogenase activity as measured by tetrazolium salt reduction. *The journal of histochemistry and cytochemistry : official journal of the Histochemistry Society.* 1960;8:296-303.

32. Old SL, Johnson MA. Methods of microphotometric assay of succinate dehydrogenase and cytochrome c oxidase activities for use on human skeletal muscle. *The Histochemical journal.* 1989;21(9-10):545-555.

33.   Schneider CA, Rasband WS, Eliceiri KW. NIH Image to ImageJ: 25 years of image analysis. *Nature methods.* 2012;9(7):671-675.

34.   McDowell EM, Trump BF. Histologic fixatives suitable for diagnostic light and electron microscopy. *Archives of pathology & laboratory medicine.* 1976;100(8):405-414.

35.   Spurr AR. A low-viscosity epoxy resin embedding medium for electron microscopy. *Journal of ultrastructure research.* 1969;26(1):31-43.

36.   De Sousa E, Veksler V, Minajeva A, et al. Subcellular creatine kinase alterations. Implications in heart failure. *Circulation research.* 1999;85(1):68-76.

37.   Estornell E, Fato R, Pallotti F, Lenaz G. Assay conditions for the mitochondrial NADH:coenzyme Q oxidoreductase. *FEBS letters.* 1993;332(1-2):127-131.

38.   Veksler VI, Kuznetsov AV, Sharov VG, Kapelko VI, Saks VA. Mitochondrial respiratory parameters in cardiac tissue: a novel method of assessment by using saponin-skinned fibers. *Biochimica et biophysica acta.* 1987;892(2):191-196.

39.   Kuznetsov AV, Veksler V, Gellerich FN, Saks V, Margreiter R, Kunz WS. Analysis of mitochondrial function in situ in permeabilized muscle fibers, tissues and cells. *Nature protocols.* 2008;3(6):965-976.

40.   Ratiney H, Albers MJ, Rabeson H, Kurhanewicz J. Semi-parametric time-domain quantification of HR-MAS data from prostate tissue. *NMR in biomedicine.* 2010;23(10):1146-1157.

41.   Wu H, Southam AD, Hines A, Viant MR. High-throughput tissue extraction protocol for NMR- and MS-based metabolomics. *Analytical biochemistry.* 2008;372(2):204-212.

42. Beauclercq S, Nadal-Desbarats L, Hennequet-Antier C, et al. Serum and Muscle Metabolomics for the Prediction of Ultimate pH, a Key Factor for Chicken-Meat Quality. *Journal of proteome research.* 2016;15(4):1168-1178.

43. Worley B, Powers R. PCA as a practical indicator of OPLS-DA model reliability. *Current Metabolomics.* 2016;4(2):97-103.

44. Xia J, Sinelnikov IV, Han B, Wishart DS. MetaboAnalyst 3.0--making metabolomics more meaningful. *Nucleic acids research.* 2015;43(W1):W251-257.

45. Kim D, Pertea G, Trapnell C, Pimentel H, Kelley R, Salzberg SL. TopHat2: accurate alignment of transcriptomes in the presence of insertions, deletions and gene fusions. *Genome biology.* 2013;14(4):R36.

46. Goecks J, Nekrutenko A, Taylor J. Galaxy: a comprehensive approach for supporting accessible, reproducible, and transparent computational research in the life sciences. *Genome biology.* 2010;11(8):R86.

47. Anders S, Pyl PT, Huber W. HTSeq--a Python framework to work with high-throughput sequencing data. *Bioinformatics (Oxford, England).* 2015;31(2):166-169.

48. Love MI, Huber W, Anders S. Moderated estimation of fold change and dispersion for RNA-seq data with DESeq2. *Genome biology.* 2014;15(12):550.

49. Chen EY, Tan CM, Kou Y, et al. Enrichr: interactive and collaborative HTML5 gene list enrichment analysis tool. *BMC bioinformatics.* 2013;14:128.

50. Kuleshov MV, Jones MR, Rouillard AD, et al. Enrichr: a comprehensive gene set enrichment analysis web server 2016 update. *Nucleic acids research.* 2016;44(W1):W90-97.

51. Picard M, McManus MJ, Csordas G, et al. Trans-mitochondrial coordination of cristae at regulated membrane junctions. *Nat Commun.* 2015;6:6259.

52. Fuchtbauer EM, Westphal H. MyoD and myogenin are coexpressed in regenerating skeletal muscle of the mouse. *Developmental dynamics : an official publication of the American Association of Anatomists.* 1992;193(1):34-39.

53. Kammoun M, Picard B, Henry-Berger J, Cassar-Malek I. A network-based approach for predicting Hsp27 knock-out targets in mouse skeletal muscles. *Comput Struct Biotechnol J.* 2013;6:e201303008.

54. Blum R, Dynlacht BD. The role of MyoD1 and histone modifications in the activation of muscle enhancers. *Epigenetics.* 2013;8(8):778-784.

55. Unger A, Beckendorf L, Bohme P, et al. Translocation of molecular chaperones to the titin springs is common in skeletal myopathy patients and affects sarcomere function. *Acta neuropathologica communications.* 2017;5(1):72.

56. Bönnemann CG. The collagen VI-related myopathies: muscle meets its matrix. *Nature reviews Neurology.* 2011;7(7):379-390.

57. Seet L-F, Toh LZ, Chu SWL, Finger SN, Chua JLL, Wong TT. Upregulation of distinct collagen transcripts in post-surgery scar tissue: a study of conjunctival fibrosis. *Disease Models & Mechanisms.* 2017;10(6):751-760.

58. DiMario JX. KLF10 Gene Expression Modulates Fibrosis in Dystrophic Skeletal Muscle. *The American journal of pathology.* 2018;188(5):1263-1275.

59. Hefferan TE, Reinholz GG, Rickard DJ, et al. Overexpression of a nuclear protein, TIEG, mimics transforming growth factor-beta action in human osteoblast cells. *The Journal of biological chemistry.* 2000;275(27):20255-20259.

60. Liu X, Joshi SK, Ravishankar B, Laron D, Kim HT, Feeley BT. Upregulation of transforming growth factor-β signaling in a rat model of rotator cuff tears. *Journal of shoulder and elbow surgery / American Shoulder and Elbow Surgeons [et al].* 2014;23(11):1709-1716.

61. Marin-Garcia J, Goldenthal MJ, Damle S, Pi Y, Moe GW. Regional distribution of mitochondrial dysfunction and apoptotic remodeling in pacing-induced heart failure. *J Card Fail.* 2009;15(8):700-708.

62. Scheubel RJ, Tostlebe M, Simm A, et al. Dysfunction of mitochondrial respiratory chain complex I in human failing myocardium is not due to disturbed mitochondrial gene expression. *Journal of the American College of Cardiology.* 2002;40(12):2174-2181.

63. Barreiro E, Puig-Vilanova E, Marin-Corral J, et al. Therapeutic Approaches in Mitochondrial Dysfunction, Proteolysis, and Structural Alterations of Diaphragm and Gastrocnemius in Rats With Chronic Heart Failure. *Journal of cellular physiology.* 2016;231(7):1495-1513.

64. Sanchez H, Zoll J, Bigard X, et al. Effect of cyclosporin A and its vehicle on cardiac and skeletal muscle mitochondria: relationship to efficacy of the respiratory chain. *Br J Pharmacol.* 2001;133(6):781-788.

65. Homedan C, Schmitt C, Laafi J, et al. Mitochondrial energetic defects in muscle and brain of a Hmbs-/- mouse model of acute intermittent porphyria. *Hum Mol Genet.* 2015;24(17):5015-5023.

66. Kollberg G, Melberg A, Holme E, Oldfors A. Transient restoration of succinate dehydrogenase activity after rhabdomyolysis in iron-sulphur cluster deficiency myopathy. *Neuromuscul Disord.* 2011;21(2):115-120.

67. Haller RG, Henriksson KG, Jorfeldt L, et al. Deficiency of skeletal muscle succinate dehydrogenase and aconitase. Pathophysiology of exercise in a novel human muscle oxidative defect. *J Clin Invest.* 1991;88(4):1197-1206.

68. Vladutiu GD, Heffner RR. Succinate dehydrogenase deficiency. *Archives of pathology & laboratory medicine.* 2000;124(12):1755-1758.

FIGURE 1 Differential gene expression analysis in the skeletal muscle of 3-month old *Tieg1* KO female mice. **A.** *Tieg1* mRNA expression levels as determined by RT-PCR in the soleus (N=5) and EDL (N=8) muscles of WT female mice. Data represent the mean ± SEM and significant differences between muscles were determined using a student's *t-test* (‡ : P < 0.001). **B.** Principal Component Analysis (PCA) and **C.** Hierarchical clustering of RNA-Seq data conducted on the soleus of WT (N=3) and *Tieg1* KO (N=3) female mice. **D.** Volcano plot of RNA-Seq data depicting differentially expressed genes in *Tieg1* KO soleus muscle compared to WT controls. Significantly down regulated genes (log2 FC < -0.8, P < 0.05) are depicted in green and up regulated genes (Log2 FC > 0.8, P < 0.05) are depicted in red.

FIGURE 2 Histochemical analysis of *Tieg1* KO (N=10) and WT (N=10) soleus muscles. Relevant muscle specific stains were performed on cross-sections of soleus muscle isolated from 3-month old *Tieg1* KO and WT female mice including SDH (**A-B**), COX (**C-D**), menadione (**E-F**), Periodic acid-Schiff (**G-H**), Oil Red O (**I-J**), and Gömöri trichrome (**K-L**).

FIGURE 3 Histochemical analysis of *Tieg1* KO (N=10) and WT (N=10) EDL muscles. Relevant muscle specific stains were performed on cross-sections of EDL muscle isolated from 3-month old *Tieg1* KO and WT female mice including SDH (**A-B**), COX (**C-D**), menadione (**E-F**), Periodic acid-Schiff (**G-H**), Oil Red O (**I-J**), and Gömöri trichrome (**K-L**).

FIGURE 4 Transmission electron microscopy analyses of soleus and EDL muscles isolated from *Tieg1* KO and WT female mice. Skeletal muscle ultrastructure was determined using TEM acquisitions of longitudinal and transverse sections of the soleus (A-F) and EDL (G-L) muscles from 3-month old *Tieg1* KO (N=7) and WT (N=7) female mice. Striking differences were observed in the I and H bands, as well as the numbers, shape and organization of mitochondria, in *Tieg1* KO muscles compared to WT controls.

FIGURE 5 Mitochondrial enzyme activities in skeletal muscle. Citrate synthase activity (A and D), complex I activity (B and E) and complex IV activity (C and F) were determined in mitochondrial preparations from soleus (A, B and C) and EDL (D, E and F) muscle isolated from 3-month old WT (N=7) and *Tieg1* KO (N=7) female mice. Data are represented as the mean ± SEM and significant differences between genotypes were determined using Mann Whitney test (* : $P < 0.05$; † : $P < 0.01$).

FIGURE 6 Mitochondrial respiratory activities in skeletal muscle. Mitochondrial complex measurements were determined from soleus (A) and EDL (B) muscle extracts of 3-month old WT (N=7) and *Tieg1* KO (N=7) female mice. Data are represented as the mean ± SEM and significant differences between genotypes were determined using Mann Whitney test (* : $P < 0.05$; † : $P < 0.01$; ‡ : $P < 0.001$).

FIGURE 7 Mitochondrial protein expression in soleus and EDL muscle. Relative expression of indicated mitochondrial proteins was determined by western blotting using soleus and EDL tissue lysates prepared from 3-month old WT (N=6) and *Tieg1* KO (N=6) female mice. Densitometry was used to quantitate protein levels and is depicted in the bar graphs for soleus (A-B) and EDL (C-D). Data are represented in arbitrary unit (A.U.) as the mean ± SEM and significant differences between genotypes were determined using Mann Whitney test († : $P < 0.01$).

FIGURE 8 Total protein carbonylation in skeletal muscle. Protein carbonylation was assessed by dot blots in protein extracts from 3-month old WT (N=6) and *Tieg1* KO (N=6) female mice. Sample types are represented as follows: wild-type soleus (WTs), wild-type EDL (WTe), Knock-out soleus (KOs) and Knock-out EDL (KOe). Densitometry was used to quantitate carbonylation levels (oxyblot) which were normalized to Coomassie B. staining

and are depicted in the bar graphs. Data are represented in arbitrary unit (A.U.) as the mean ± SEM and no significant differences were detected.

FIGURE 9 ^{1}H spectral analysis of skeletal muscle. (**A**) In vivo hindlimb muscle ^{1}H spectra from 3-month old WT (N=12) and *Tieg1* KO (N=12) female mice. Creatine, taurine and extracellular lipids are represented by 1, 2 and 3 respectively. (**B-C**) Muscle metabolites using ^{1}H in vivo spectroscopy quantified in arbitrary unit (A.U.).

Choline (cho), creatine (cre), taurine (tau) and extracellular lipids (emlc) are depicted. Values from WT mice are represented by white boxplots and *Tieg1* KO mice are represented by blue boxplots.

FIGURE 10 ^{31}P spectral analysis of skeletal muscle. (**A**) In vivo hindlimb muscle ^{31}P spectra from 3-month old WT (N=12) and *Tieg1* KO (N=12) female mice. Inorganic phosphate, phosphocreatine, ATPγ, ATPα and ATPβ are represented by 1, 2, 3, 4 and 5 respectively. (**B**) Muscle metabolites using ^{31}P in vivo spectroscopy quantified in arbitrary unit (A.U.). Inorganic phosphate (Ip), phosphocreatine (PCr), ATPγ, ATPα and ATPβ are depicted. Significant differences between muscle genotypes were determined using Mann Whitney test (* : $P < 0.05$; † : $P < 0.01$).

FIGURE 11 Principal Component Analysis (PCA) of the ^{1}H-NMR spectral data. WT soleus (3 spectra from N=18 muscles, purple circles), *Tieg1* KO soleus (3 spectra from N=18 muscles, blue circles), WT EDL (3 spectra from N=18 muscles, yellow circles) and *Tieg1* KO EDL (3 spectra from N=18 muscles, red circles) are shown.

FIGURE 12 Metabolic analysis of soleus and EDL muscles. Heatmaps are represented to depict differentially regulated metabolites in the soleus and EDL muscles of 3-month old WT and *Tieg1* KO female mice (N=18) generated from ^{1}H-NMR spectral features. Up-regulated

(red) and down-regulated (blue) metabolites in the *Tieg1* KO muscles are shown relative to WT controls.

FIGURE 13 Treadmill exercise test of endurance. Three month old WT (N=15) and *Tieg1* KO (N=15) female mice were subjected to a treadmill exercise test. Mice were run to exhaustion and the total distance run (m) was recorded. Data are represented as the mean ± SEM and significant differences between genotypes was determined using a Mann Whitney test (‡ : $P < 0.001$).
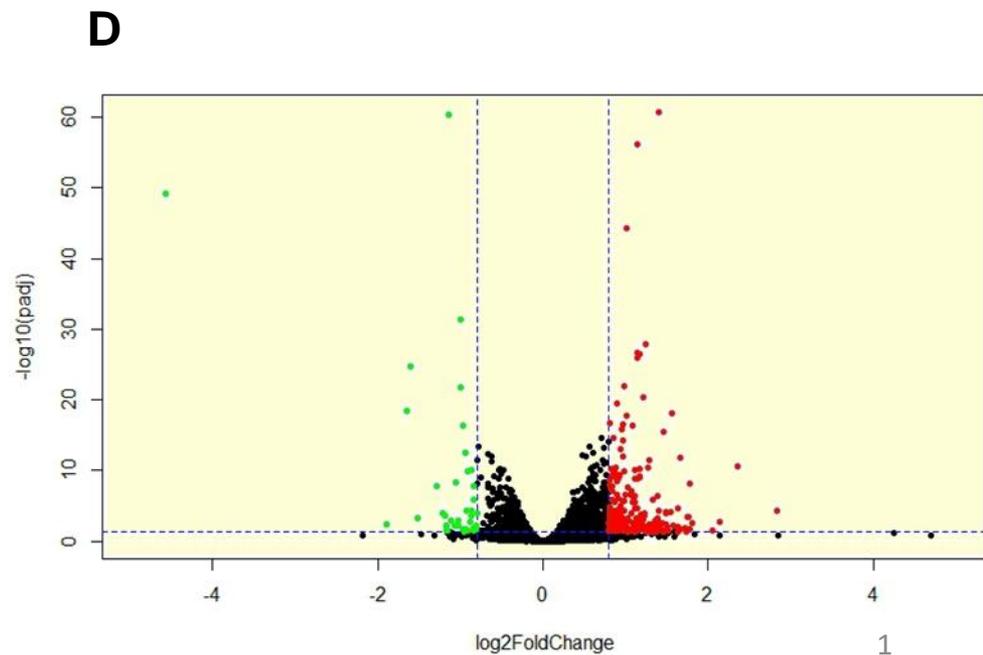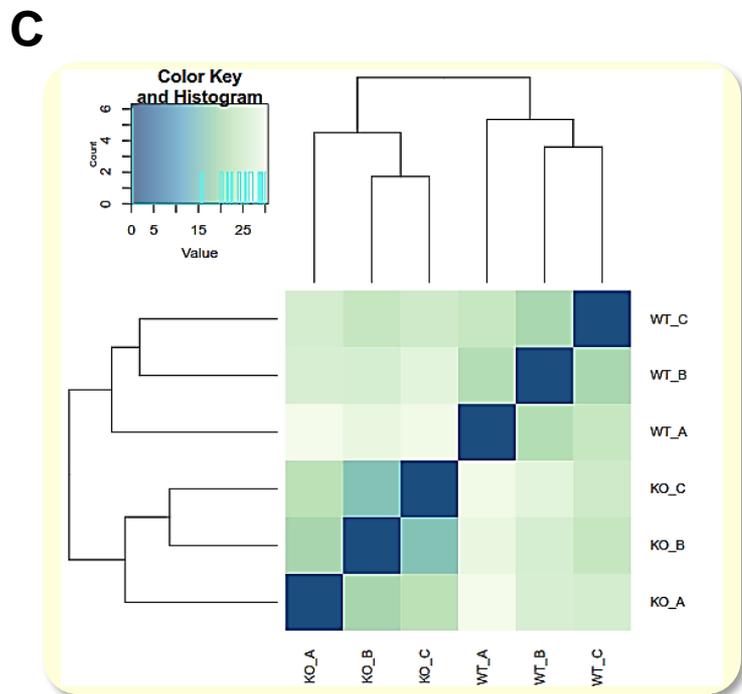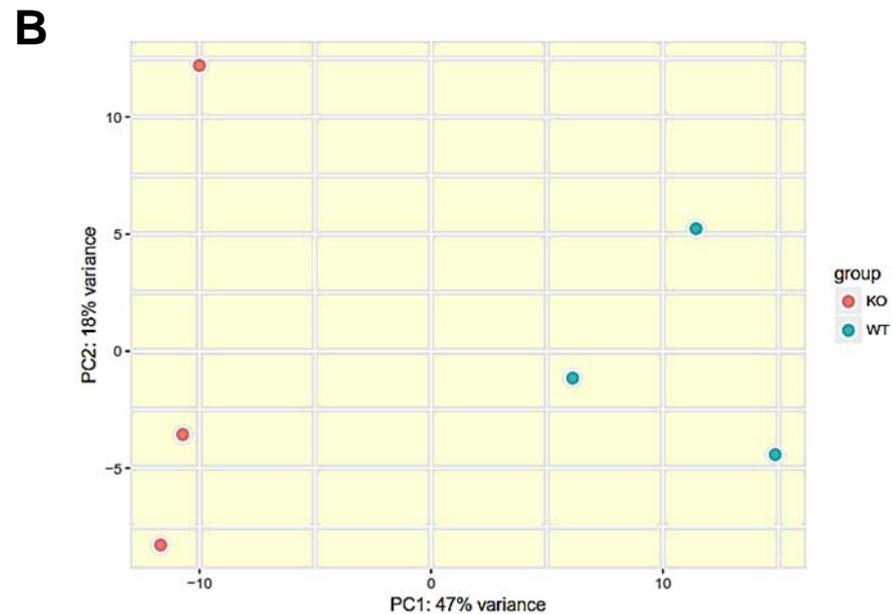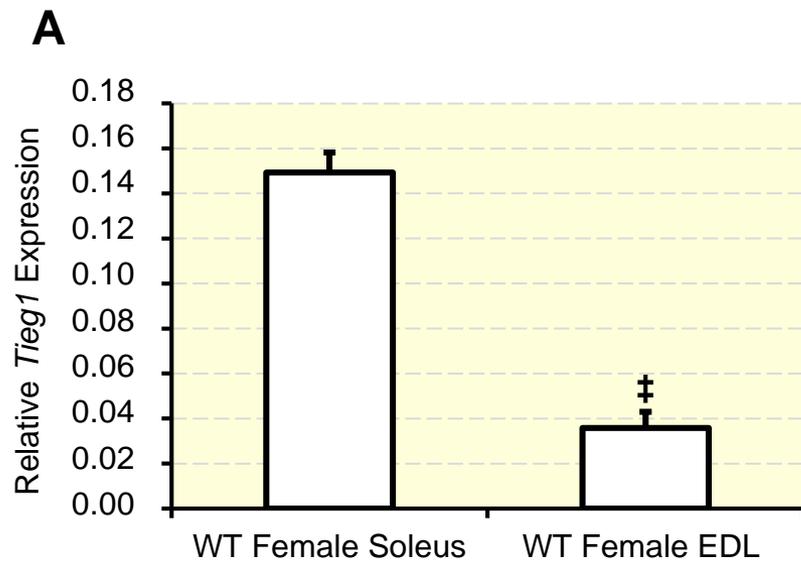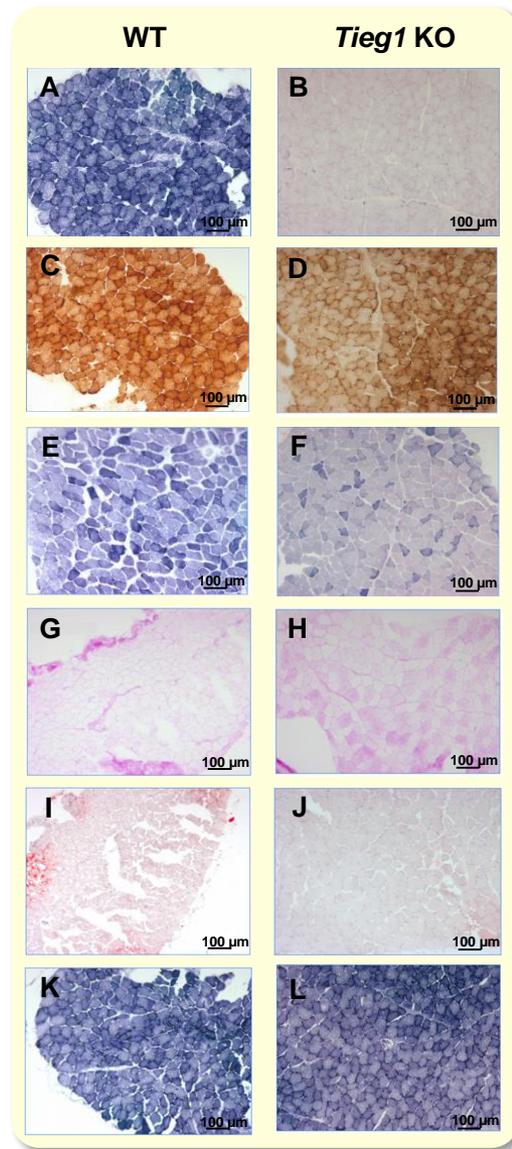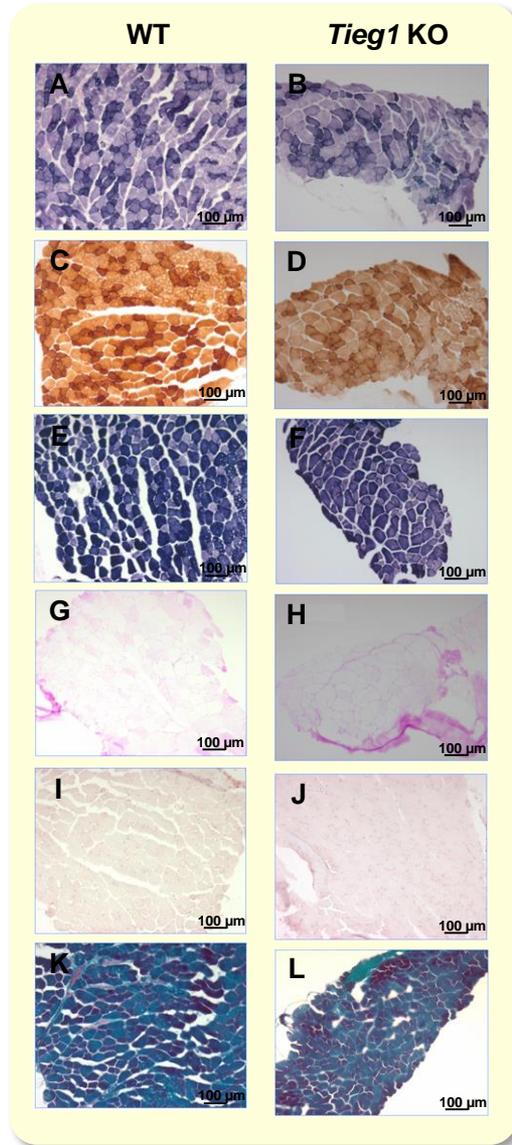
A

B

C

D

1

WT	Tieg1 KO
A	B
C	D
E	F
G	H
I	J
K	L

| | WT | Tieg1 KO |

A — Sol WT
H band
2.5 µm
I band
Mitochondria
2 µm

B
Mitochondria
500 nm

C
Myosin
200 nm

D — Sol *Tieg1* KO
1.5 µm
Mitochondria
2 µm

E
Mitochondria
500 nm

F
Myosin
200 nm

G — EDL WT
H band
2.5 µm
I band
Mitochondria
2 µm

H
Mitochondria
500 nm

I
Myosin
200 nm

J — EDL *Tieg1* KO
1.5 µm
Mitochondria
2 µm

K
Inclusion
Affected Mitochondria
500 nm

L
Myosin
200 nm
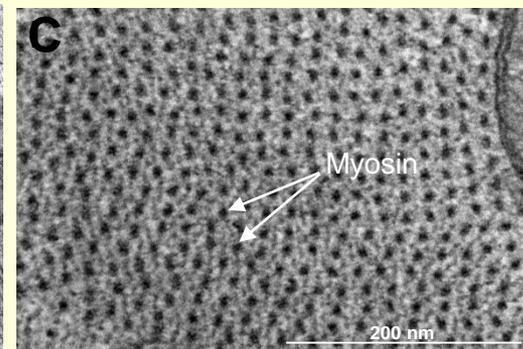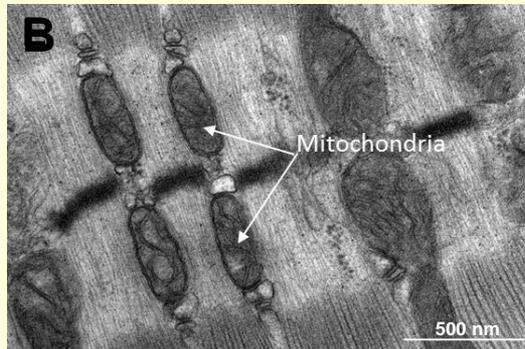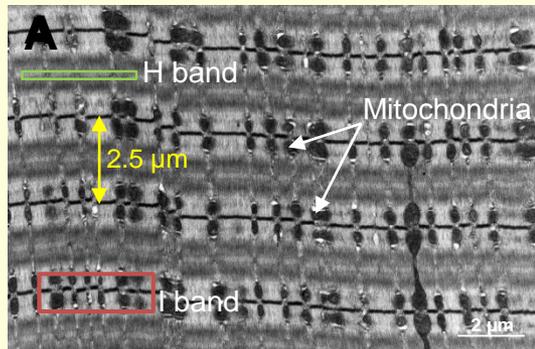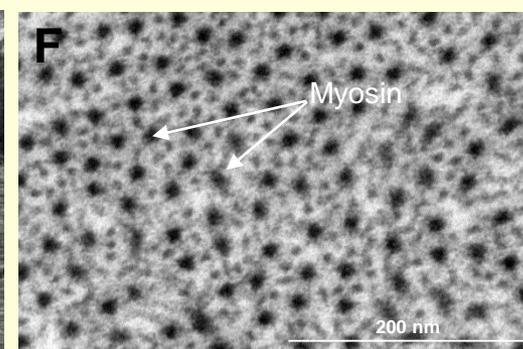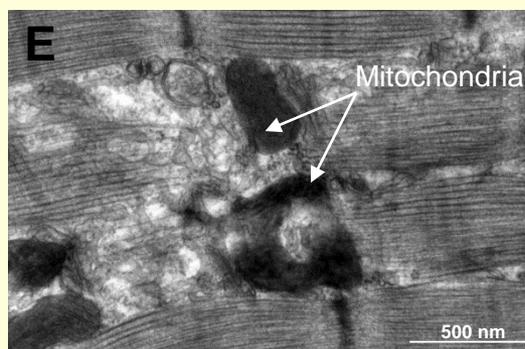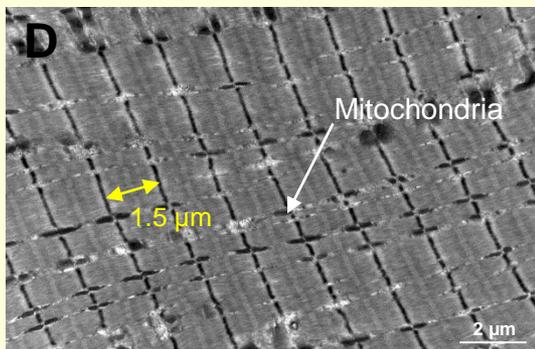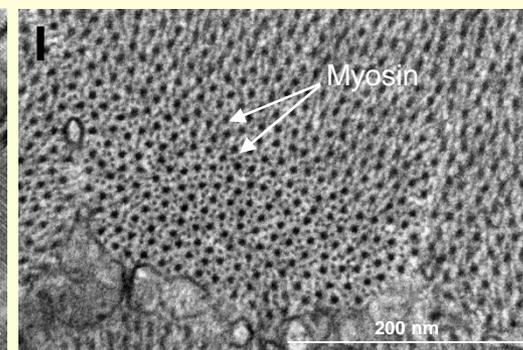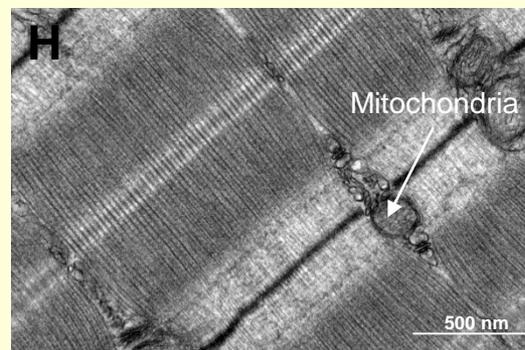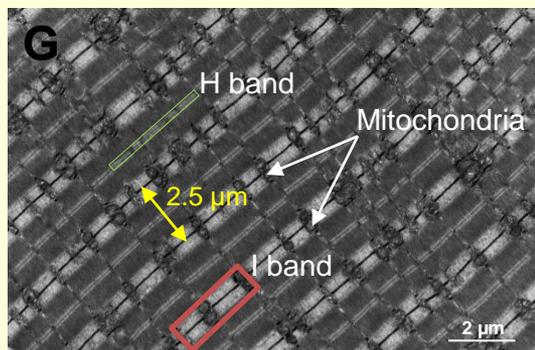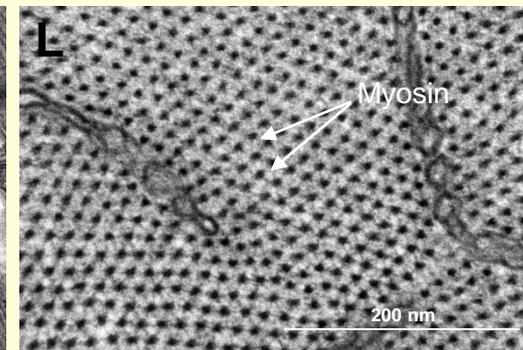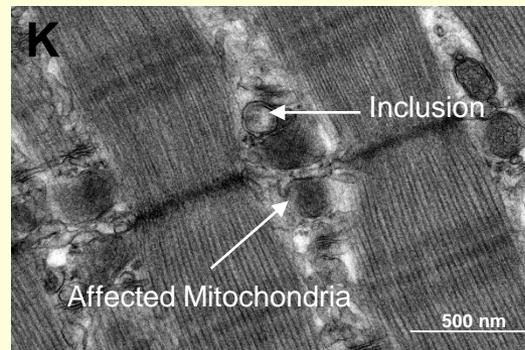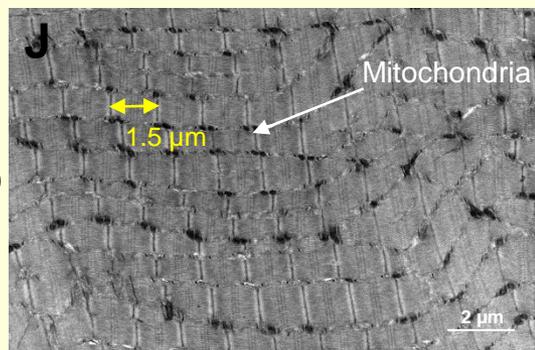
Citrate synthase activity
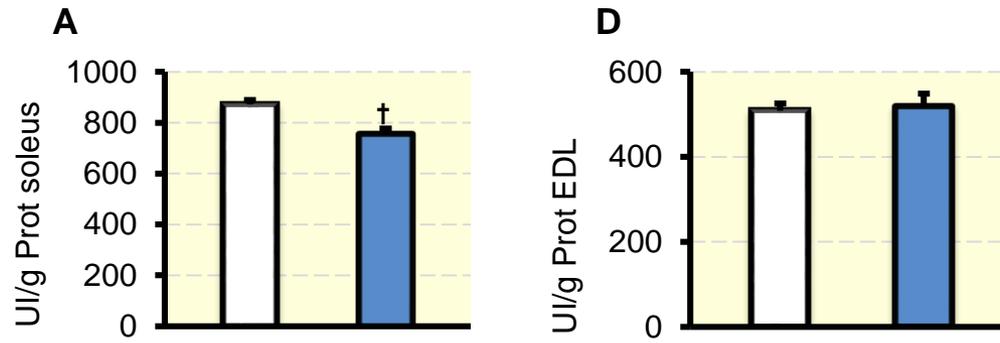
Complex I activity

Complex IV activity

Soleus

A

(X10³)

C-V
C-III
C-II
C-I
Vinculin

WT   Tieg1 KO

EDL

C

(X10³)

C-V
C-III
C-II
C-I
Vinculin

WT   Tieg1 KO

B

(X10³)

Cox4
Vinculin
CS
Vinculin
Mfn2
Vinculin
PGC-1a
Vinculin
DRP1
Actin
OPA1
Actin

WT   Tieg1 KO

D

(X10³)

Cox4
Vinculin
CS
Vinculin
Mfn2
Vinculin
PGC-1a
Vinculin
DRP1
Actin
OPA1
Actin

WT   Tieg1 KO

☐ WT   ■ Tieg1 KO

7

Oxyblot

WTs KOs WTe KOe

Coomassie B.

WTs KOs WTe KOe

Oxyblot (protein carbonylation)

Protein carbonylation (A.U.) Normalized to Coomassie B.

soleus   EDL

☐ WT   ■ *Tieg1* KO

A

WT
Tieg1 KO

3

1

2 2 1

[ppm]

B

¹H muscle MRS

A.U.

80000
70000
60000
50000
40000
30000
20000
10000
0

cho   cho   cre   cre   tau   tau

C

¹H muscle MRS

A.U.

800000
700000
600000
500000
400000
300000
200000
100000
0

emlc   emlc

WT   *Tieg1* KO

9

A

WT
Tieg1 KO

1

2

3

4

5

20   10   0   -10   -20   -30   [ppm]

B   **^{31}P muscle MRS**

(X10^3)

3

2

1

0

A.U.

*

†

Ip   PCr   ATPγ   ATPα   ATPβ

☐ WT   ◼ *Tieg1* KO

10

A soleus

WT   *Tieg1* KO

B EDL

Spectrum

#1   #2   #3

VIP

Nicotinurate
Tyrosine
Glutamine
Glutamate
Valine
Leucine
B-711
Lysine/Cadaverine
B-HO-Butyrate
Leucine/Isoleucine

Up regulated

Down regulated

1.5
1
0.5
0
-0.5
-1
-1,5

Spectrum

#1   #2   #3
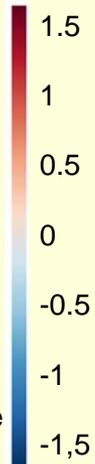
VIP

Nicotinurate
Fumarate
Lactate
Pyruvate
Aspartate
Valine
Glutamate
Leucine/Isoleucine
B-HO-Butyrate
Lysine/Cadaverine
Ala/Glu/Gln
Phenylalanine

Up regulated

Down regulated

12